Smart Structures and Systems, *Vol. 29, No. 2 (2022) 301-309*
https://doi.org/10.12989/sss.2022.29.2.301

Corrosion visualization under organic coating using laser ultrasonic propagation imaging

Anseob Shin [1,2], Jinhwan Park [1,3], Heesoo Lee [4], Yunshil Choi [5] and Jung-Ryul Lee*[5]

[1] *Korea Coating Technology Center, Pukyong National University, Busan, Republic of Korea*
[2] *School of Convergence Science, Pusan National University, Busan, Republic of Korea*
[3] *Department of Industrial Chemistry, Pukyong National University, Busan, Republic of Korea*
[4] *School of Materials Science and Engineering, Pusan National University, Busan, Republic of Korea*
[5] *Department of Aerospace Engineering, Korea Advanced Institute of Science and Technology, Daejeon, Republic of Korea*

(*Received March 22, 2021, Revised July 14, 2021, Accepted October 19, 2021*)

Abstract. Protective coatings are most widely used anticorrosive structures for steel structures. The corrosion under the coating damages the host material, but this damage is completely hidden. Therefore, a field-applicable under-coating-corrosion visualization method has been desired for a long time. Laser ultrasonic technology has been studied in various fields as an in situ nondestructive inspection method. In this study, a comparative analysis was carried out between a guided-wave ultrasonic propagation imager (UPI) and pulse-echo UPI, which have the potential to be used in the field of under-coating-corrosion management. Both guided-wave UPI and pulse-echo UPI were able to successfully visualize the corrosion. Regarding the field application, the guided-wave UPI performing Q-switch laser scanning and piezoelectric sensing by magnetic attachment exhibited advantages owing to the larger distance and incident angle in the laser measurement than those of the pulse-echo UPI. Regarding the corrosion visualization methods, the combination of adjacent wave subtraction and variable time window amplitude mapping (VTWAM) provided acceptable results for the guided-wave UPI, while VTWAM was sufficient for the pule-echo UPI. In addition, the capability of multiple sensing in a single channel of the guided-wave UPI could improve the field applicability as well as the relatively smaller size of the system. Thus, we propose a guided-wave UPI as a tool for under-coating-corrosion management.

Keywords: coating; corrosion visualization; G-UPI (Guided wave- Ultrasonic Propagation Imager); nondestructive; PE-UPI (Pulse-Echo Ultrasonic propagation Imager)

1. Introduction

In steel bridges and metal structures, coatings are applied as a barrier to isolate metal structures from corrosive environments. Protective coatings are the most common anticorrosive techniques for steel structures (Sangaj and Malshe 2004, Shin and Shon 2010). However, only qualitative evaluations have been carried out through visual inspections observing rust, peeling, checking, and chalking (Construction Technology Digital Library 2020, Lee *et al*. 2009). In the case of super-structures in the field, quantitative condition evaluation of the structure is not possible owing to the problems of accessibility and evaluation of large areas. The corrosion under the coating damages the host material, but this damage is completely hidden. In the field, technologies that can be used to quantitatively measure and visualize the degree of corrosion under an organic coating are required for maintenance and structural integrity management.

Therefore, a field-applicable under-coating-corrosion visualization method has been desired for a long time. Nondestructive ultrasonic wave imaging technologies are being studied in various fields in the aerospace, airplane, defense, and nuclear industries, which require high reliability and safety (Lee *et al*. 2019, Choi *et al*. 2018, Gan *et al*. 2019, Yang *et al*. 2015, Liu *et al*. 2020, Majhi *et al*. 2021, James *et al*. 2021). In addition, recent studies on the visualization of corrosion sites under organic coatings are being studied using Ultrasonic Time-Domain Reflectometry and IR-thermography (Kot *et al*. 2021, Sliem *et al*. 2021, Bi *et al*. 2021, Yang *et al*. 2018, Schmitt *et al*. 2017). The study of laser ultrasonic technology, which has no effect on the liquid medium and thermal influence and can be measured in the field, is attracting attention.

The inspection method using the ultrasonic generation laser enables noncontact inspection without coupling medium for scanning and can provide highly reliable experimental results through the advantages of reduced inspection time by the high scanning speed and receiving ultrasonic waves in the point-per-point area. This is an effective method for damage visualization and detection of damage locations. Although methods for such damage visualization and damage location detection have been reported, few studies have evaluated the corrosion under organic coatings. In other words, the evaluation of the corrosion under the coating while it is used in the field is in the beginning stage.

*Corresponding author, Professor,
E-mail: leejrr@kaist.ac.kr

ISSN: 1738-1584 (Print), 1738-1991 (Online)

In this study, a comparative analysis was carried out between a guided-wave ultrasonic propagation imager (UPI) and pulse-echo UPI, which have the potential for use in the field of under-coating-corrosion management. For making conclusion, we focused on three of considerations:

- Visualization of under-coating-corrosion: Confirm that the inspection system is able to present reasonable visualization result for under-coating-corrosion.
- Field applicability: Based on scanning mechanism, confirm applicability of the systems on large super-structures.
- Accuracy: To confirm accuracy of the results, conduct shape comparison between visualization results and actual corrosion on the specimen.

2. Corrosion Visualization using UPIs

2.1 Damage visualization algorithms for UPIs

In this study, a comparative evaluation was carried out to study the possibility of visualizing corrosion evaluation under an organic coating by applying guided-wave and pulse-echo UPIs. The UPIs irradiate laser beams to generate ultrasonic waves on the structure. The ultrasonic waves are captured by contact or noncontact sensors. As shown in Fig. 3(a), the UPIs are classified into two different configurations, guided-wave UPI, which uses a contact-type sensor and laser mirror scanner (LMS) for beam steering, and pulse-echo UPI, which uses a noncontact-type sensor and linear translation stages for excitation and sensing laser beam positioning. The guided-wave UPI uses a guided wave, whereas the pulse-echo UPI uses bulk waves. In the case of the guided-wave UPI, all ultrasonic signals have different arrival times because the distance between the excitation point and sensor location changes. On the other hand, excitation and sensing lasers, i.e., laser Doppler vibrometer (LDV), in the pulse-echo UPI are always shifted together. Thus, all ultrasonic signals have the same arrival times when the target structure is homogeneous. Ultrasonic wave signals, which represent A-scan signals, are stacked into a three-dimensional array (space × space × time) while scanning, as shown in Fig. 3(b). Ultrasonic wave propagation imaging (UWPI), a default output of the UPI, provides a video clip result generated using C-scan representations as time frames of the video clip, which shows the wave propagation pattern with time.

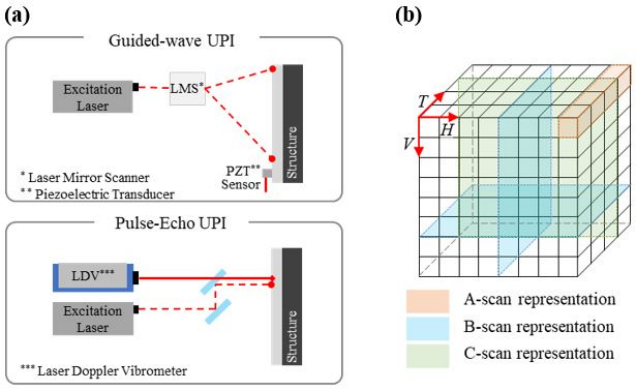

Fig. 1 (a) UPIs; and (b) scanning data representation

The variable time window amplitude mapping (VTWAM) (Fig. 2), the easiest image processing technique in the UPI systems converts three-dimensional data into a two-dimensional image. The time window in which damage including an anomalous wave is visible in the raw signal or post-processed signal is selected, which is the result of expressing the signal magnitude in the time window as a color intensity map. A typical amplitude mapping is different from mapping an image of the entire time window to the maximum amplitude. However, the VTWAM technique selects and maps an image in a specific time window in which the damage area appears, which leads to improved corrosion visualization results compared to the general amplitude map (Choi and Lee 2017).

2.2 Experimental setup

As depicted in Fig. 3, the corroded surface was prepared using 5% NaCl on a carbon steel with a thickness of 3 mm,

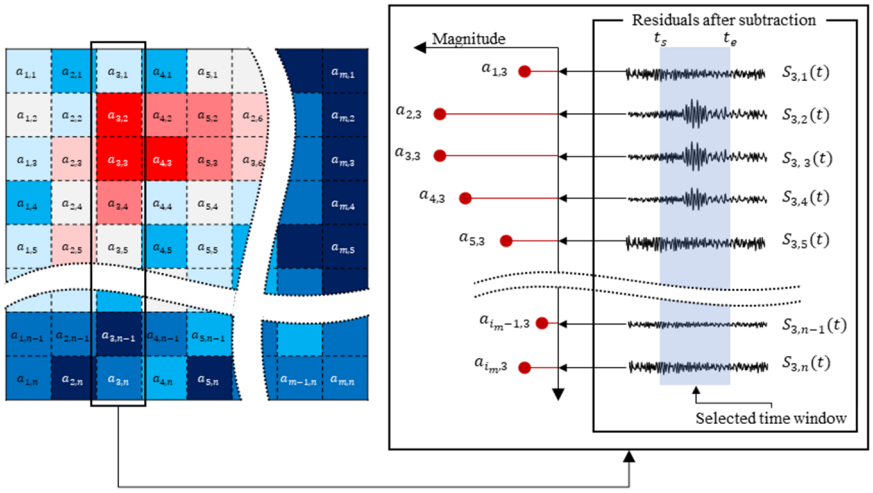

Fig. 2 Schematic of the VTWAM

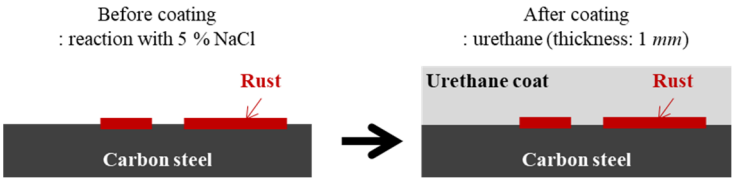

Fig. 3 Schematic of the specimen

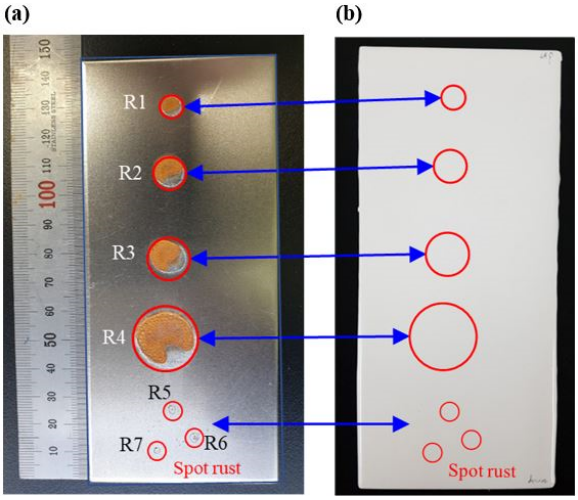

Fig. 4 Appearances (a) before and (b) after the coating of the corrosion specimen

and then a urethane coating for corrosion protection was applied to a thickness of approximately 1 mm. Fig. 4 shows the corrosion specimen before and after the coating. Before the coating, areal type of rusts (R1, R2, R3 and R4) were induced within various diameters of 5 mm to 21 mm, and spot rusts (R5, R6 and R7) with diameter of approximately 0.5 mm were also induced together as shown in Fig. 4(a). The specimen after the coating shown in Fig. 4(b), all the rusts were totally covered with the urethane coat, thus these rusts were not able to be evaluated via visual testing anymore.

Fig. 5 shows the setting of the actual specimen using the guided-wave UPI. The inspection conditions are listed in Table 1. Ultrasonic signals were induced by a Nd:YLF ($\lambda = 1053$ nm) laser with an excitation energy (E) of 1.5 mJ and

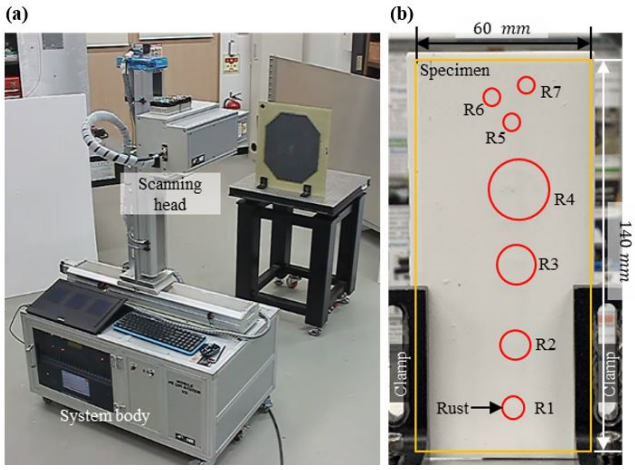

Fig. 6 Photographs of the (a) pulse-echo UPI equipment; and (b) experimental setup for the specimen

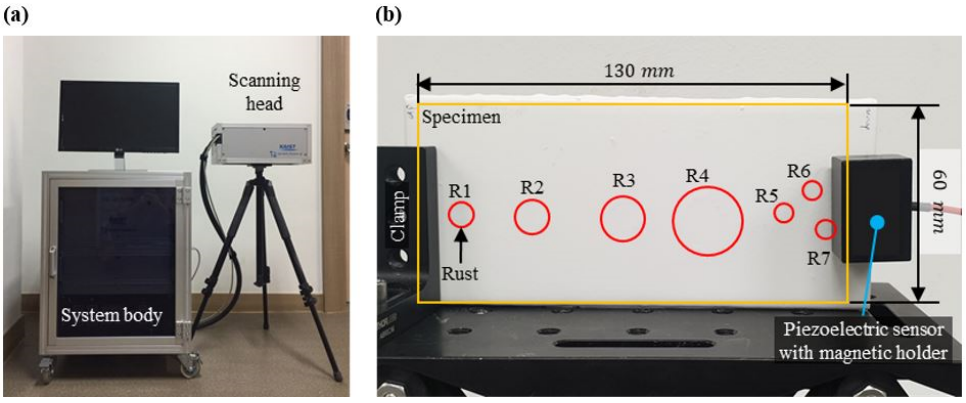

Fig. 5 Photographs of the (a) guided-wave UPI; and (b) experimental setup for the specimen

Table 1 Experimental conditions for the guided-wave UPI

Transmitter	Nd:YLF ($\lambda = 1053$ nm) / $E = 1.5$ mJ / $f_{PRF} = 5$ kHz
Receiver	Amplifier-integrated PZT sensor with a magnetic holder installation
Scanning information	Area: 130×60 mm^2 / Interval: 0.25 mm / Stand-off distance: 651 mm
Data acquisition	Band-pass filter range: 170 − 900 kHz with a gain of 4 / $f_s = 3$ MHz

Table 2 Experimental conditions for the pulse-echo UPI

Transmitter	Nd:YAG ($\lambda = 1064$ nm) / $E = 2.7$ mJ / $f_{PRF} = 1$ kHz
Receiver	LDV ($\lambda_{LDV} = 633$ nm, 20 mm/s/V)
Scanning information	Area: 60×140 mm^2 / Interval: 0.1 mm / Stand-off distance: 483 mm
Data acquisition	Band-pass filter range: $250 - 500$ kHz / $f_s = 60$ MHz

pulse repetition frequency (PRF, f_{PRF}) of 5 kHz. All ultrasonic signals were captured using an amplifier-integrated piezoelectric sensor with a magnetic installation mount and were digitized to 16-bit discrete signals with a sampling rate (f_s) of 3 MHz after conditioning through a programmable band-pass filter with a band-pass range of $170 - 900$ kHz.

Fig. 6 shows a photograph of the appearance of the pulse-echo UPI and specimen evaluation, while Table 2 shows the inspection conditions. The main components of the pulse-echo UPI are a Nd:YAG laser ($\lambda = 1064$ nm) as an ultrasonic generator and LDV ($\lambda_{LDV} = 633\,nm$) as a receiver, with a PRF of 1 kHz and band-pass filter frequency of 250 to 500 kHz.

3. Results and discussion

3.1 Guided-wave UPI

Fig. 7 shows freeze-frames of UWPI video clip results at $94\,\mu s$ and VTWAM results with a selected time window of 50 to $160\,\mu s$, based on the guided-wave UPI. As the amplifier-integrated PZT sensor was located on the right side of the scan area, the UWPI results show propagation from right to left. The VTWAM results also show a considerably larger magnitude distribution on the right side of the scan area, because the guided waves attenuate as the travel distance increases. In the freeze-frame and VTWAM results obtained using broad-band analog filtered data shown in Figs. 7(a) and (b), the corrosion areas are not clearly visualized. An additional narrow-band numerical filtering was applied to the inspection results to enhance the visibility of the under-coating rust. A fourth-order Butterworth filter was designed and applied to all time domain signals and UWPI video clip and VTWAM results were generated again. Figs. 7(c) and (d) show freeze-frames of UWPI and VTWAM results after applying the narrow-band numerical filter. The freeze-frame of the UWPI still shows a low visibility. However, according to the VTWAM results in Fig. 7(d), the corrosion areas at R1–R4 are visualized with a higher visibility than that in Fig. 7(b).

The visualization of the under-coating corrosion on the specimen was confirmed as shown in Fig. 7, and data investigation and review were carried out for the other signal processing methods. The UPI systems are equipped several processing algorithms to provide better convenience of damage evaluation. One of the processing algorithms in the UPI systems, ultrasonic energy map (UEM) performs two-dimensional FFT for spatial domain and extracts specific wavenumber components which are amplified by structural anomalies. (Joh *et al*. 2021) UEM technique especially has been applied to various applications and has been proved its reliability in many of studies. However, UEM and VTWAM techniques require extra input parameters such as wavenumber, bandwidth and time window, thus inspection quality might be varied depending on training level of inspectors. The other technique in the UPI systems, referred as adjacent wave subtraction (AWS) algorithm attenuates incident waves by analyzing waveform

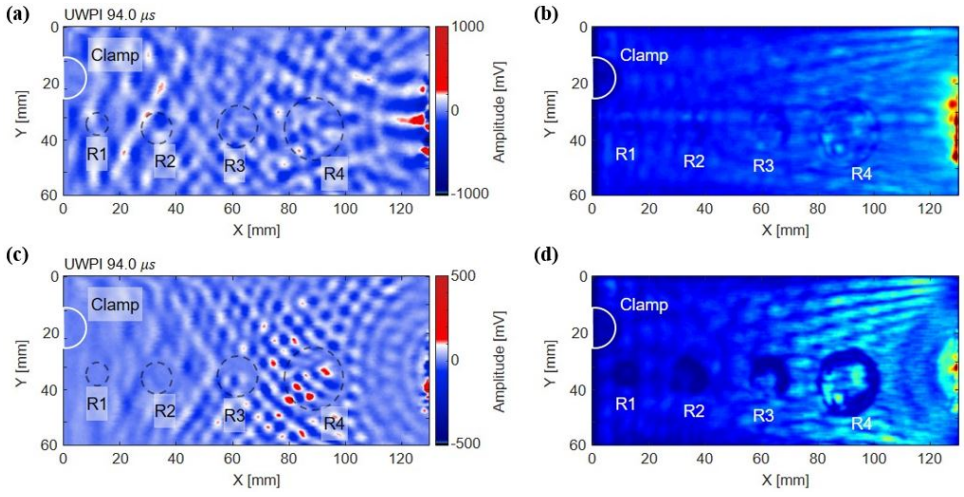

Fig. 7 Results of the guided-wave UPI with broad-band analog filtering, (a) freeze-frame of the UWPI at $94\,\mu s$; (b) VTWAM (time window: $50 - 160\,\mu s$) and with broad-band analog filtering + narrow-band numerical filtering (fourth-order Butterworth filter, $420 - 480$ kHz); (c) freeze-frame of the UWPI at $94\,\mu s$; and (d) VTWAM (time window: $50 - 160\,\mu s$)

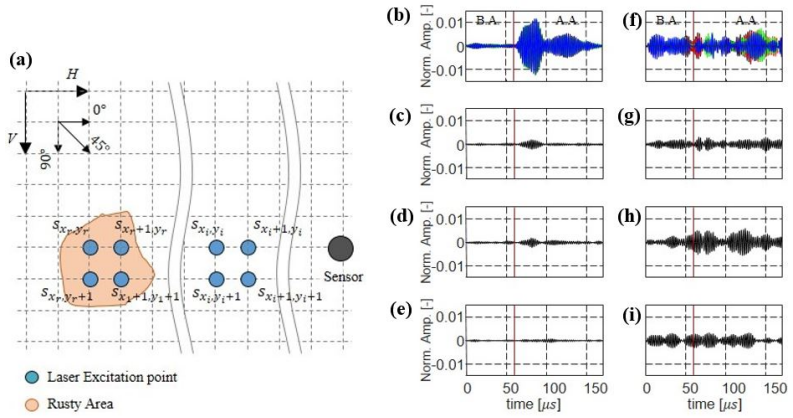

Fig. 8 (a) Schematic of adjacent waves locations; (b) ultrasonic signal of $S_{35.5,43}$ and its adjacent signals and residuals after AWS processing at (c) 0; (d) 45; and (e) 90°; and (f) ultrasonic signal of $S_{35.5,38.5}$ and its adjacent signals and residuals after AWS processing at (g) 0; (h) 45; and (i) 90°

similarities with neighborhood to provide greater damage visibility and easy of time window selection for VTWAM. The AWS technique compares two adjacent signals and carries out time window adjustment and subtraction of the posterior signal with respect to time to achieve maximum similarity between the adjacent signals. In other words, the aforementioned technique enhances the damage visibility by removing the incident wave with a larger amplitude and amplifying the anomalous wave with a lower amplitude. The ultrasonic signals obtained from two adjacent laser irradiation points are very similar, and the residuals after the time window adjustment and subtraction exhibit amplitudes similar to the noise level. When the subtraction is performed using signals guided from the damage point or near the damage point, a confining wave or scattering wave amplified by a mismatch of the phase appears. Multi-directional AWS (Choi and Lee 2017), which is an advanced AWS technique, uses posterior signals along various directions. The conventional AWS technique uses a posterior signal along the horizontal axis of the scan area. However, the multi-directional AWS technique can selectively use adjacent waves in different directions, as shown in Fig. 8(a).

Figs. 8(b) to (i) show the ultrasonic signals obtained from the results in Fig. 7(c). Fig. 8(b) shows the ultrasonic signals extracted from the coordinates of [35.5:35.75, 43:43.25], which are in the intact region. All signals have high similarities. The residuals after AWS processing shown in Figs. 8(c) and (d) also show that the incident waves were attenuated successfully. On the other hand, ultrasonic signals extracted from the coordinates of [35.5:35.75, 38:38.75], which are in the rust area (Fig. 8(f)), have low similarities. The residuals after the AWS processing shown in Figs. 8(g) to (i) also show higher amplitude levels than those in Figs. 8(c) and (d). In the above results, the first norm values (l_1) of the residuals were compared to select the optimum AWS processing direction. As shown in Table 3, the l_1 values from the residuals of the intact region are smaller than those from the residuals of the rust area. Although the l_1 value of the residual after the AWS processing at 45° is larger than those of the others, the ratio between the l_1 values of the residuals from the intact and rust areas is maximized in the case of 90° AWS processing. This implies that the damage visibility at 90° of the AWS-processed result was maximized. Thus, we discussed only the AWS results processed at 90°.

Fig. 9 shows the AWS-processed results at 90°, using the signals obtained by applying the Butterworth filter in the range of 420 to 480 kHz. The urethane coating yielded a rapid attenuation of ultrasonic signals. Thus, all signals were normalized before the AWS processing with the first norm of each signal to ensure visibility of all rust areas in an image result. Figs. 9(a) and (b) show freeze-frame of AWPI at $94\,\mu s$ and VTWAM generated using the result shown in Fig. 9(a) with time range of $50-160\,\mu s$. As compare to the above results in Fig. 7(d), most of incident wave components have been eliminated, and boundaries of rust areas have been highlighted successfully by relatively amplified anomalous wave components.

To select appropriate time window for VTWAM, inspectors should observe video clip results and specify time window based on their opinions. Due to that AWS processing attenuates incident waves and relatively amplifies anomalous waves, inspectors are able to select proper time window much easily with greater visibility of anomalous waves. However, because of the characteristics

Table 3 First norm values of the residuals

AWS processing direction	Intact region ($l_{1,i}$)	Rust area ($l_{1,r}$)	Ratio ($l_{1,r}/l_{1,i} \times 100$ [%])
0°	0.1605	0.5270	328.35%
45°	0.1959	0.8401	428.84%
90°	0.1154	0.5927	513.60%

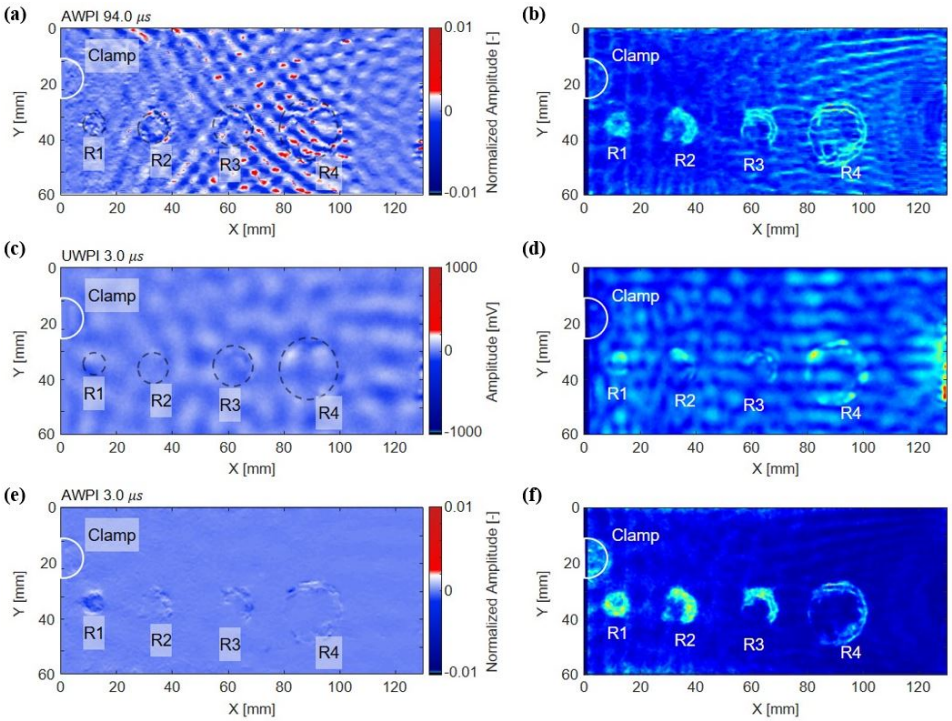

Fig. 9 (a) Freeze-frame of AWPI video clip at $94.0\ \mu s$; (b) VTWAM with AWS-processed signals (time range: $50\ \mu s - 160\ \mu s$); (c) freeze-frame of UWPI video clip at $3.0\ \mu s$; (d) VTWAM with narrow band-pass filtered signals (time range: $0\ \mu s - 45\ \mu s$); (e) freeze-frame of AWPI video clip result at $3.0\ \mu s$; and (f) VTWAM with AWS-processed signals (time range: $0\ \mu s - 45\ \mu s$)

of the G-UPI, that having different arrival times of all signals on each grid point by changes of traveling distance between excitation and sensing points, a specified time window for generating VTWAM might be not able to secure visibilities of damages in one time if the scan area is too large. To select much appropriate time window regardless to size of scan area and arrival times, specific time window "before arrival time" is able to be selected in alternative. Delamination between urethane coating and surface of structure and wall-thinning caused by surface rust induce standing waves which are not attenuated and keep being scattered within the boundaries of damaged area. These standing waves keep being resident till next laser impingement is implemented, thus the standing waves referred as reverberation, superposed on noise window is able to be observed (Joh *et al*. 2021). Damage visualization using AWS-processing with reverberation effect is conducted as following:

i. Induce reverberation artificially using high pulse repetition frequency (i.e., very fast laser scanning, above 3 kHz or higher)
ii. Apply narrowband numerical bandpass filters and normalization for all time domain signals
iii. Implements AWS-processing
iv. Generate VTWAM using reverberation window

As shown in Figs. 8(b) and (f), amplitude levels within reverberation window ($t < 60\ \mu s$) show dramatic difference depending on the presence or absence of rust. Furthermore, AWS-processed signal shown in Fig. 8(i) shows greater amplitude level than that shown in Fig. 8(e). As shown in a freeze-frame of the UWPI video clip result in Figs. 9(c) and (d), rust areas are already visualized by reverberation. The results after AWS-processing presented in Figs. 9(e) and (f), a freeze-frame of AWPI video clip at $3.0\ \mu s$ and VTWAM with time window of $0\ \mu s$ to $45\ \mu s$ show greater visibilities for all the rust area. Compared to the VTWAM result in Fig. 9(d), the higher magnitude around the sensor location was removed, and only anomalous waves induced by the corrosion (Beena *et al*. 2017, Olisa *et al*. 2021) were emphasized. This implies that we can use a particular time window before the arrival time for the generation of the VTWAM. The spot rusts were not visualized. It is thought that the spot rusts have not given rise to thickness loss. However, visualization of the target corrosions could be confirmed based on the processing technique. The AWS and VTWAM techniques are considered superior to signal processing for the improvement in the corrosion visualization.

3.2 Pulse-echo UPI

Fig. 10 shows the freeze-frame of the UWPI video obtained using the bulk-wave pulse-echo UPI. The corrosion can be observed in the video. The corrosion areas are clearly visible in the VTWAM.

Fig. 11 compares the results of the guided-wave UPI and pulse-echo UPI after exposing metal areas by coating removal (KCC, YY900) to re-verify the corrosion area under the organic coating. Fig. 11(a) shows that the rust formed on the metal specimen was transferred to the bottom

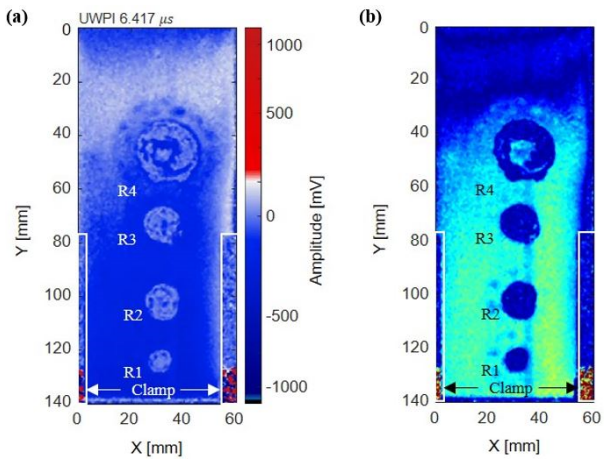

Fig. 10 Results of the pulse-echo UPI: (a) freeze-frame of the UWPI video clip at $6.417\ \mu s$; and (b) VTWAM (time window: $6.083 - 6.183\ \mu s$)

of the coating, while Fig. 11(b) shows the rust formed on the upper part of the metal specimen. The shape of the corrosion area was changed (grown) compared to the initial stage. Figs. 11(c) and (d) show the guided-wave UPI and pulse-echo UPI results, respectively. Both results visualize not only the corrosion areas under the organic coating, but also the growth and deformation. In Fig. 11(d), the pulse-echo UPI result shows a more similar shape. Additionally, to further clarify the corrosion area, the particle morphology and constituents of the specimen were observed using environmental scanning electron microscopy (E-SEM) and energy-dispersive X-ray spectroscopy (EDS), as shown in Fig. 12. The results confirmed that the area with Fe and O as the major rust constituents agrees with the area visualized by the UPIs.

Table 4 summarizes the visualization results for the corrosion area under the organic coating obtained using the guided-wave and pulse-echo UPIs. According to the above results, both guided-wave UPI and pulse-echo UPI can be used for nondestructive inspections and rust visualization of organic-coated structures. The pulse-echo UPI results exhibited a higher accuracy than that of the guided-wave UPI results. The field applicability of the guided-wave UPI is better than that of the pulse-echo UPI because the beam steering manner equipped on the guided-wave UPI provides a considerably simplified usage and smaller portable size of the system. In the case of the pulse-echo UPI, the size of the capable scan area depends on the dimensions of the linear translation stages, which are used for positioning of the scanning head of the pulse-echo UPI. However, the LMS equipped on the scanning head of the guided-wave UPI provides a larger scan area than that of the linear-scan pulse-echo UPI. Furthermore, the scanning head of the pulse-echo UPI has a limited scan speed because the laser and LDV head always move together by linear translation stages. However, the LMS, which maneuvers using Galvano motors, can perform a considerably faster laser scanning with a PRF of tens of kilohertz (Joh *et al*. 2021). In conclusion, both guided-wave and pulse-echo UPIs were able to visualize the corrosion area under the organic coating. The guided-wave UPI is excellent in terms of field applicability.

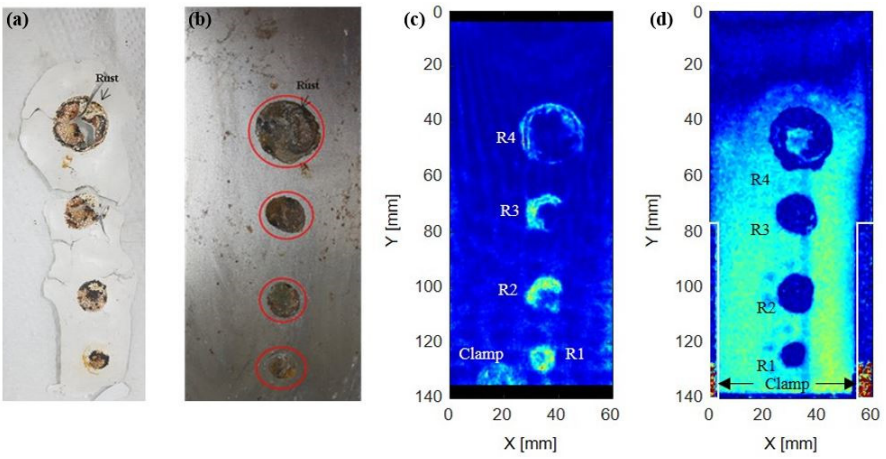

Fig. 11 Coating removal for verification. (a) Bottom of the coating; (b) Top of the steel specimen. Results of the VTWAM obtained by the (c) guided-wave UPI; and (d) pulse-echo UPI

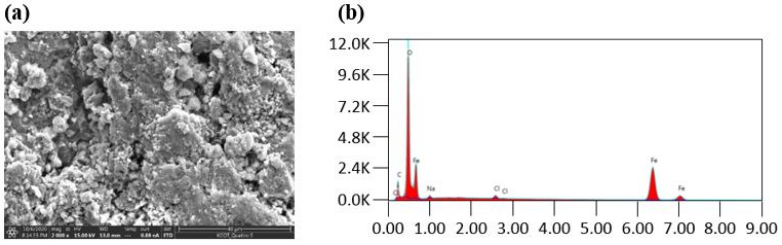

Fig. 12 Rust area (a) E-SEM image; and (b) EDS profile

Table 4 Comparison of the guided-wave UPI and pulse-echo UPI

Properties	Angular-scan guided-wave UPI	Linear-scan pulse-echo UPI	Properties
Visualization of corrosion areas under the organic coating	Possible	Possible	Visualization of corrosion areas under the organic coating
Field applicability	Excellent	Limited application	Field applicability
Accuracy	Accurate	More accurate	Accuracy

4. Conclusions

In this study, we investigated the visualization of corrosion under an organic coating using a guide-wave UPI and pulse-echo UPI. The results of this study can be summarized as follows.

- Both guided-wave and pulse-echo UPIs were able to successfully visualize the corrosion under the organic coating.
- Regarding the field application, the guided-wave UPI performing Q-switch laser scanning and piezoelectric sensing by magnetic attachment exhibited advantages owing to the larger distance and incident angle in the laser measurement than those of the pulse-echo UPI.
- Regarding the corrosion visualization methods, the combination of AWS and VTWAM provided acceptable results for the guided-wave UPI, while VTWAM was sufficient for the pule-echo UPI.

Acknowledgments

This study was supported by a research grant from the Korea Evaluation Institute of Industrial Technology (20010566).

References

Beena, K., Shruti, S., Sandeep, S. and Naveen, K. (2017), "Monitoring degradation in concrete filled steel tubular sections using guided waves", *Smart Struct. Syst.*, *Int. J.*, **19**(4), 371-382. https://doi.org/10.12989/sss.2017.19.4.371

Bi, H., Weinell, C.E., de Pablo, R.A., Varela, B.S., Carro, S.G., Ruiz, Á.R. and Dam-Johansen, K. (2021), "Rust creep assessment—A comparison between a destructive method according to ISO 12944 and selected non-destructive methods", *Prog. Org. Coat.*, **157**, 106293. https://doi.org/10.1016/j.porgcoat.2021.106293

Choi, Y. and Lee, J.R. (2017), "Multi-directional adjacent wave subtraction and shifted time point mapping algorithms and their application to defect visualization in a space tank liner", *NDT & E Int.*, **86**, 53-64. https://doi.org/10.1016/j.ndteint.2016.11.009

Choi, Y., Abbas, S.H. and Lee, J.R. (2018), "Aircraft integrated structural health monitoring using lasers, piezoelectricity, and fiber optics", *Measurement*, **125**, 294-302. https://doi.org/10.1016/j.measurement.2018.04.067

Construction Technology Digital Library (2020), Standard Specifications for Road & bridges Works, Republic of Korea.

Gan, C.S., Tan, L.Y., Chia, C.C., Mustapha, F. and Lee, J.R. (2019), "Nondestructive detection of incipient thermal damage in glass fiber reinforced epoxy composite using the ultrasonic propagation imaging", *Funct. Compos. Struct.*, **1**(2), 025006-025016. https://doi.org/10.1088/2631-6331/ab260a

Institute of Civil Engineering and Building Technology, Goyang-si, Republic of Korea. https://www.codil.or.kr

James, V., Carswell, D., Riise, J., Nicholson, P.I., Graf, N., Huber, N., Gärtner, M., Reitinger, B., Scherleitner, E., Burgholzer, P. and Phipps, J. (2021), "Robot deployed Laser-Ultrasonic NDT system for inspection of large aircraft structures", *IOP Conference Series*: *Materials Science and Engineering*, **1024**, 012032. https://10.1088/1757-899X/1024/1/012032

Joh, J., Choi, Y. and Lee, J.R. (2021), "Reverberation-based high-speed guided-wave ultrasonic propagation imager for structural inspection of thick composites", *Compos. Struct.*, **259**, 1113446-1113460. https://doi.org/10.1016/j.compstruct.2020.113446

Kot, P., Muradov, M., Gkantou, M., Kamaris, G.S., Hashim, K. and Yeboah, D. (2021), "Recent Advancements in Non-Destructive Testing Techniques for Structural Health Monitoring", *Appl. Sci.*, **11**, 2750. https://doi.org/10.3390/app11062750

Lee, C.Y., Lee, S.H. and Park, J.H. (2009), "Evaluation of Deterioration of Epoxy Primer for Steel Bridge Coating using Image Processing and Electrochemical Impedance Spectroscopy", *Corros. Sci. Tech.*, **8**(2), 53-61.

Lee, W.J., Seo, B.H., Hong, S.C., Won, M.S. and Lee, J.R. (2019), "Real world application of angular scan pulse-echo ultrasonic propagation imager for damage tolerance evaluation of full-scale composite fuselage", *Struct. Health Monitor.*, **18**(5-6), 1943-1952. https://doi.org/10.1177/1475921719831370d

Liu, P., Jang, J. and Sohn, H. (2020), "Crack localization by laser-induced narrowband ultrasound and nonlinear ultrasonic modulation", *Smart Struct. Syst.*, *Int. J.*, **25**(3), 301-310. https://doi.org/10.12989/sss.2020.25.3.301

Majhi, S., Mukherjee, A., George, N.V., Karaganov, V. and Uy, B. (2021), "Corrosion monitoring in steel bars using Laser ultrasonic guided waves and advanced signal processing", *Mech. Syst. Sig. Proc.*, **149**, 107176. https://doi.org/10.1016/j.ymssp.2020.107176

Olisa, S.C., Khan, M.A. and Starr, A. (2021), "Review of Current Guided Wave Ultrasonic Testing (GWUT) Limitations and Future Directions", *Sensors*, **21**(3), 811. https://doi.org/10.3390/s21030811.

Sangaj, N.S. and Malshe, V.C. (2004), "Permeability of polymers in protective organic coatings", *Prog. Org. Coat.*, **50**(1), 28-39. https://10.1016/j.porgcoat.2003.09.015

Schmitt, G., Lenzmann, C., Schneider, N. and Lobnig, R. (2017), "Non-destructive indication of delaminations under thick organic coatings using active IR-thermography", *Mater. Corros.*, **68**, 1285-1294. https://doi.org/10.1002/maco.201609333

Shin, A. and Shon, M. (2010), "Effects of coating thickness and surface treatment on the corrosion protection of diglycidyl ether bisphenol-A based epoxy coated carbon steel", *J. Ind. Eng. Chem.*, **16**(6), 884-890. https://doi.org/10.1016/j.jiec.2010.09.016

Sliem, M.H., Fayyad, E.M., Abdullah, A.M., Younan, N.A., Al-Qahtani, N., Nabhan, F.F., Ramesh, A., Laycock, N., Ryan, M.P., Maqbool, M. and Arora, D. (2021), "Monitoring of under deposit corrosion for the oil and gas industry", *J. Pet. Sci. Eng.*,

204, 108752. https://doi.org/10.1016/j.petrol.2021.108752
Yang, J., Liu, P., Yang, S., Lee, H. and Sohn, H. (2015), "Laser based impedance measurement for pipe corrosion and bolt-loosening detection", *Smart Struct. Syst.*, *Int. J.*, **15**(1), 41-55. https://doi.org/10.12989/sss.2015.15.1.041
Yang, R., He, Y., Zhang, H. and Huang, S. (2018), "Through coating imaging and nondestructive visualization evaluation of early marine corrosion using electromagnetic induction thermography", *Ocean Eng.*, **147**, 277-288. https://doi.org/10.1016/j.oceaneng.2017.09.023

HJ